Geophysical Research Letters

RESEARCH LETTER
10.1029/2025GL120749

Tropical Cyclones Drive Enhanced Inorganic Iodine in the Mid-Latitude Upper Troposphere

Karolin Voss[1], Bärbel Vogel[2], Thorsten Diederich[3], Andreas Engel[3], Jens-Uwe Grooß[2], Timo Keber[3], Flora Kluge[1,4], Meike K. Rotermund[1,5], Tanja Schuck[3], Benjamin Weyland[1], André Butz[1,6,7], and Klaus Pfeilsticker[1,6]

[1]Institute of Environmental Physics, Universität Heidelberg, Heidelberg, Germany, [2]Institute of Climate and Energy Systems—Stratosphere (ICE-4), Forschungszentrum Jülich, Jülich, Germany, [3]Institute for Atmospheric and Environmental Science, Goethe University Frankfurt, Frankfurt, Germany, [4]Now at: ECMWF, Bonn, Germany, [5]Now at: Department of Physics, University of Toronto, Toronto, ON, Canada, [6]Heidelberg Center for the Environment, Heidelberg University, Heidelberg, Germany, [7]Interdisciplinary Center for Scientific Computing, Heidelberg University, Heidelberg, Germany

Abstract Halogens deplete tropospheric and stratospheric ozone, but the role of iodine is still elusive. Atmospheric iodine mainly originates from marine inorganic (I_2, HOI) and organic (CH_3I, CH_2I_2, CH_2IBr, and CH_2ICl) emissions. We report on airborne measurements of atmospheric iodine oxide (IO) concentrations up to 15 km altitude from two flights of the WISE campaign over the mid-Atlantic in September and October 2017. IO is retrieved from limb scattered skylight in the upper troposphere (UT) using the airborne mini-DOAS instrument on board the German High Altitude and LOng range research aircraft (HALO). Elevated IO (maximum 0.58 ppt, mean 0.36 ± 0.08 ppt over 2.5 hr) was observed in the UT in air masses processed by category 5 hurricanes Irma and Maria. Our findings show that enhanced IO mixing ratios are driven by fast vertical transport through tropical cyclones and potentially enhanced marine iodine emissions due to associated high surface winds.

Plain Language Summary Halogen gases can destroy ozone. However, the role of iodine in ozone destruction is not well understood. The main source of iodine is the ocean. Using a research aircraft, we measured gaseous iodine oxide over the Atlantic Ocean during two flights in the autumn of 2017. Our observations of elevated amounts of iodine oxide in air masses influenced by hurricanes Irma and Maria in the mid-latitude upper troposphere show that fast vertical transport lifted iodine-rich air masses to the upper troposphere, potentially supported by enhanced marine iodine emissions due to strong hurricane surface winds.

Key Points:

- Enhanced IO mixing ratios (maximum 0.58pptv, mean 0.36 ± 0.08pptv) detected in hurricane-processed air in the mid-latitude upper troposphere
- Hurricane-driven transport lifted iodine-rich air masses from the tropical marine boundary layer into the mid-latitude upper troposphere
- The source region of iodine-rich air coincides with two hurricanes, suggesting elevated oceanic emissions due to strong surface winds

Supporting Information:

Supporting Information may be found in the online version of this article.

Correspondence to:

K. Voss and K. Pfeilsticker,
karolin.voss@uni-heidelberg.de;
Klaus.pfeilsticker@iup.uni-heidelberg.de

Citation:

Voss, K., Vogel, B., Diederich, T., Engel, A., Grooß, J.-U., Keber, T., et al. (2026). Tropical cyclones drive enhanced inorganic iodine in the mid-latitude upper troposphere. *Geophysical Research Letters*, *53*, e2025GL120749. https://doi.org/10.1029/2025GL120749

Received 24 NOV 2025
Accepted 3 MAY 2026

Author Contributions:

Conceptualization: Karolin Voss, André Butz, Klaus Pfeilsticker
Formal analysis: Karolin Voss
Funding acquisition: André Butz, Klaus Pfeilsticker
Investigation: Karolin Voss, Bärbel Vogel, Thorsten Diederich, Andreas Engel, Jens-Uwe Grooß, Timo Keber, Flora Kluge, Meike K. Rotermund, Tanja Schuck
Methodology: Karolin Voss
Project administration: Klaus Pfeilsticker
Supervision: André Butz, Klaus Pfeilsticker
Visualization: Karolin Voss

1. Introduction

Halogens (Cl, Br, and I) are known to deplete both tropospheric and stratospheric ozone (WMO, 2022). Compared to chlorine, the ozone depletion potential on a per atom basis is around 60 to 75 times larger for bromine and 150 to 300 times larger for iodine (Engel et al., 2018; Klobas et al., 2021; Ko et al., 2003; Sinnhuber et al., 2009). In the troposphere, iodine additionally influences the oxidative capacity by affecting the HO_x to NO_x ratio (Bloss et al., 2005) and may form ultra-fine aerosol particles (Finkenzeller et al., 2023; He et al., 2021; Huang et al., 2022; O'Dowd et al., 2002; Saiz-Lopez et al., 2014).

The dominant source of atmospheric iodine is the ocean. In contrast to oceanic bromine sources, more than half of the iodine emitted by the ocean is in inorganic form (I_2 and HOI) with a smaller contribution of organic iodine emissions, in particular CH_3I, with even smaller contributions from other iodinated very short lived substances (VSLS) (e.g., CH_2I_2, CH_2IBr, and CH_2ICl) (WMO, 2022). Non-oceanic sources of atmospheric iodine are generally episodic and include the release from mineral dust (Koenig et al., 2021; Reza et al., 2024), volcanic emissions (Aiuppa et al., 2005), the release from sea ice (Atkinson et al., 2012; Saiz-Lopez et al., 2015), terrestrial biogenic sources (Sive et al., 2007), biomass burning (Schill et al., 2025), and anthropogenic sources (Wu et al., 2014). An efficient pathway of inorganic iodine emission from the ocean was first described by Carpenter et al. (2013), and its emission strength has recently been updated by Pound et al. (2024). Inorganic iodine emissions are driven by the reaction of ozone with iodide (I^-) in the sea surface microlayer. They are largely dependent on wind speed, marine boundary layer (MBL) ozone concentrations, sea surface temperature, salinity,

Writing – original draft: Karolin Voss, Klaus Pfeilsticker
Writing – review & editing: Karolin Voss, Bärbel Vogel, Thorsten Diederich, Andreas Engel, Jens-Uwe Grooß, Meike K. Rotermund, Tanja Schuck, Benjamin Weyland, André Butz, Klaus Pfeilsticker

and availability of I^- in the sea surface micro-layer. Organic iodine emissions mainly originate from marine biological activity and also depend on wind speed (Quack & Wallace, 2003; Ziska et al., 2013).

I_2 and HOI photolyze within minutes (Bauer et al., 1998; Saiz-Lopez et al., 2004), releasing iodine atoms (I), which are then quickly oxidized by O_3 to form IO. A steady state between I and IO is reached rapidly during daytime through the photolysis of IO and the reaction of I with O_3, thus they are often collectively termed active iodine IO_x (Saiz-Lopez et al., 2012). While CH_3I has a tropospheric lifetime of 3.5–14 days (WMO, 2022) dominated by its photolysis rate, other organic iodine source gases have even shorter tropospheric lifetimes. Gaseous IO_x sinks include the reaction with HO_2 to HOI, NO to INO_2, or NO_2 to $IONO_2$, the reaction to higher iodine oxides (IO_y), or iodine containing oxoacids HIO_x (Finkenzeller et al., 2023), the latter two forming particles. Aerosol uptake of HOI, HI, INO_2, $IONO_2$ and their reactions with dissolved halide ions and stimulation by oxidized organics may initiate release of halogens to the gas phase (ICl, IBr, I_2 and others) (Finkenzeller et al., 2023; Huang et al., 2022; Koenig et al., 2020; Q. Li et al., 2022; Moon et al., 2025; Reza et al., 2024). Physical loss processes of gas phase and particulate iodine include wet scavenging of soluble species, and dry or wet aerosol deposition (Badia et al., 2019; Moon et al., 2025; Saiz-Lopez et al., 2012, 2014; Simpson et al., 2015).

The atmospheric budget of total iodine is still poorly constrained due to the low abundance of iodine outside the MBL, variable sources in space and time, and its partitioning into several species in the gas and particulate phase. As discussed by Saiz-Lopez et al. (2012), several organic and inorganic iodinated species have been measured within the MBL with in situ and remote sensing methods. However, only a handful of species have been successfully measured outside the MBL at few locations around the globe. In particular, gaseous inorganic iodine in the troposphere and stratosphere has been constrained by a few measurements of IO through differential optical absorption spectroscopy (DOAS) (e.g., Bösch et al., 2003; Butz et al., 2009; Dix et al., 2013; Koenig et al., 2020, 2021; Pundt et al., 1998; Volkamer et al., 2015; Wittrock et al., 2000). In the free troposphere (FT) and upper troposphere (UT) over the tropical Eastern Pacific Ocean, Dix et al. (2013) and Volkamer et al. (2015) measured IO volume mixing ratios (VMRs) around (0.1 ± 0.1) ppt using airborne DOAS measurements. Koenig et al. (2020) reported on (0.06 ± 0.03) ppt of IO and particulate iodine $I_{y,part}$ from which they concluded that total iodine $I_y = (0.77 \pm 0.10)$ ppt is present in the lowermost stratosphere (LMS). Further, Schill et al. (2025) reported on the widespread presence of iodine in non-sea-salt aerosols and typically $\sim$0.1 ppt in the UT with increasing VMRs in the LMS over the mid-latitude Atlantic.

The main open issues of current research on atmospheric iodine are its sources and their strengths, its tropospheric and stratospheric abundance, and its spatiotemporal variability as well as its transport pathways into the UT and stratosphere. This information is still limited due to sparse coverage of measurements outside the MBL (Lee et al., 2024), specifically in extratropical regions. Thus, the global and regional impact of atmospheric iodine is uncertain and, at present, only a few chemical transport models (CTMs) consider its atmospheric photochemistry (e.g., CAM-Chem (Saiz-Lopez et al., 2023)).

Tegtmeier et al. (2013) discussed the potential for iodine-rich air masses to be transported into the UT/LMS by tropical cyclones based on MBL CH_3I measurements and forward air mass trajectories. Here, we report on elevated IO concentrations with respect to the UT background detected during two flights of the WISE (Wave-driven ISentropic Exchange) campaign over the mid-Atlantic in autumn of 2017. The enhancements can be traced back to the influence of the hurricanes Maria and Irma in the tropical Atlantic using the Chemical Lagrangian Model of the Stratosphere (CLaMS) (McKenna, Konopka, et al., 2002; McKenna, Grooß, et al., 2002; Pommrich et al., 2014, and references therein). IO abundances are retrieved from limb scattered skylight collected by the mini-DOAS instrument (Hüneke et al., 2017) from aboard the German High Altitude and LOng range research aircraft (HALO). Rotermund et al. (2021) and Lauther et al. (2022) previously discussed the influence of vertical transport by these hurricanes on concentrations of brominated gases and chlorocarbons in the UT/LMS during the WISE campaign.

2. Data and Methods

The present study reports on limb scattered skylight measurements analyzed by the mini-DOAS instrument (Hüneke et al., 2017), which was deployed aboard the HALO aircraft during the WISE campaign in autumn of 2017. The WISE campaign was based in Shannon, Ireland, and research flights led into the European sector of the mid-Atlantic. The main interest of the campaign was to probe extratropical air to investigate transport processes

around the UT/LMS. During the campaign, remnant air masses of the category 5 hurricanes Irma and Maria were transported toward Europe and investigated during some flights. More details on the campaign and discussed flights are described in Schäfler et al. (2021), Rotermund et al. (2021), Lauther et al. (2022), and others within the special issue (https://acp.copernicus.org/articles/special_issue1061.html).

2.1. Aircraft Observations

The mini-DOAS remote sensing instrument is an assembly of six optical spectrometers for the UV, VIS, and NIR spectral ranges operating in nadir and limb view (Hüneke, 2016; Hüneke et al., 2017). Here, we use the UV ($310 - 440$ nm) and VIS ($425 - 640$ nm) spectrometers pointing starboard from the HALO aircraft, collecting limb-scattered skylight. The retrieval of IO VMRs at flight altitude follows three critical steps: (a) retrieve slant column densities (SCDs) of IO from the absorption spectra using the DOAS (Differential Optical Absorption Spectroscopy) technique (Stutz & Platt, 1996); (b) reference the IO SCDs to those of a gas with known abundance and vertical distribution, in our case O_4 (collisional oxygen complex), and rescale by the known concentration of the reference to account for the length of the light path to first order (Hüneke et al., 2017; Stutz et al., 2017); (c) correct higher order light path effects such as those caused by differences in vertical distribution of the target and reference gases and by spectrally variable scattering properties using a radiative transfer model, in our case McArtim (Monte Carlo atmospheric radiative transfer model) (Deutschmann et al., 2011). The details of these steps are outlined in the Supporting Information S1. The procedure has been validated for various gases against independent measurements and models (Hüneke, 2016; Hüneke et al., 2017; Kluge et al., 2020, 2023; Rotermund et al., 2021; Weyland et al., 2025).

Our remote sensing measurements are sensitive to a large volume of air since the collected photons travel through the atmosphere along various paths and the observed absorption stems from a composite of these light paths. Typical mean limb photon path lengths within the IO spectral window range from about 20 km when the aircraft flies in the lower troposphere to about 80 km in the UT. To estimate the averaging volume for each observation, we calculate the photon paths through the vertical layers of the atmosphere using McArtim and convolve these photon paths with the instrument's field-of-view and the horizontal distance traveled by the aircraft during spectra acquisition (see Supporting Information S1 for details).

As supportive data sets, we use in situ O_3 measurements by the FAIRO instrument (Zahn et al., 2012) and bromocarbon measurements by the GhOST (Gas chromatograph for Observational Studies using Tracers, Keber et al. (2020)) instrument aboard the HALO aircraft.

2.2. Chemical Lagrangian Model of the Stratosphere (CLaMS)

For the interpretation of our measurements the Lagrangian CTM CLaMS is used (McKenna, Konopka, et al., 2002; McKenna, Grooß, et al., 2002; Pommrich et al., 2014, and references therein) which was developed with the aim of studying transport and chemical processes in the UT/LMS. In general, it includes stratospheric chlorine and bromine chemistry (Grooß et al., 2025), but lacks iodine chemistry. In our study, CLaMS is used to analyze the origin of the sampled air masses using back trajectories as well as 3-dimensional global CLaMS simulations using the concept of surface-origin tracers (Vogel et al., 2019, 2026). Furthermore, forward-trajectories are calculated to infer a possible later entry of enhanced I_y into the LMS.

CLaMS diabatic back- and forward trajectories driven by ERA5 reanalysis data (Hersbach et al., 2020) with high resolution (0.3° latitude × 0.3° longitude and 1 hr) were initiated for the research flights on 27 September 2017 and 1 October 2017 (Clemens et al., 2024; Vogel et al., 2024). For each IO observation, 20 start positions for the trajectory calculations were distributed within the averaging volume of the observation. Back trajectories were calculated until 30 days prior to the IO observations or until they reached the CLaMS boundary layer. From the same start positions, 14-d forward-trajectories were also calculated.

Three-dimensional CLaMS simulations which include irreversible mixing (Konopka et al., 2007) provide a very good representation of observed tracer gradients in the UT/LMS. Here, we use global CLaMS simulations with different regional surface-origin tracers that are released in the CLaMS boundary layer (approximately 2–3 km above the surface, accounting for orography) every 24 hr and are subsequently transported into the free atmosphere over the course of the simulation (Vogel et al., 2019, 2026). This simulation was started on 1 May 2017 and was driven by ERA5 reanalysis data with a 1.0° × 1.0° horizontal resolution and a 6-hr time resolution (Ploeger

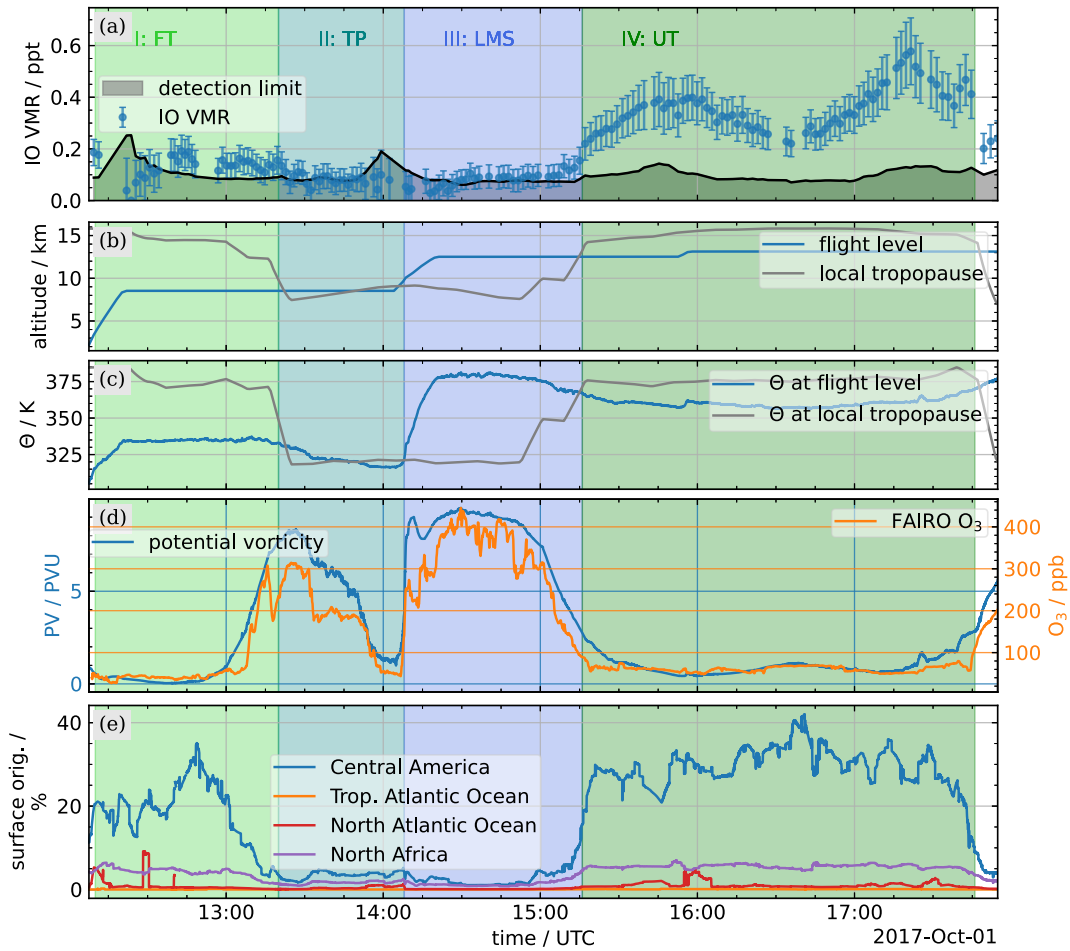

Figure 1. Overview of (a) retrieved IO VMRs and detection limits, (b) flight and tropopause altitude, (c) potential temperatures Θ at flight level and the tropopause, (d) potential vorticity (PV) and O_3, and (e) surface-origin tracer fractions along the flight track for the flight on 1 October 2017. The timeseries is subdivided into four sections depending on the probed altitude relative to the tropopause: FT (I), tropopause (II), LMS (III), and UT (IV). For a definition of the surface-origin tracers refer to Figure S2 in Supporting Information S1.

et al., 2021). The results of the simulation as well as the local tropopause, calculated from ERA5 reanalysis data based on the WMO definition according to Hoffmann and Spang (2022), are interpolated in space and time along the HALO aircraft flight tracks.

3. Results

IO VMRs are retrieved for all sunlit flight sections of the WISE campaign. For most flights, the detected IO spectral signals are below or around the detection limit, which is generally around 0.1 ppt. However, the flight on 1 October 2017 yields enhanced and robust IO SCDs between 15:16 and 17:46 UTC (peak: $SCD_{IO} = (4.4 \pm 0.7) \cdot 10^{13}$ molec cm^{-2} at 17:42 UTC). In this time span, inferred IO SCDs translate into an average IO VMR of (0.36 ± 0.08) ppt with a range between (0.22 ± 0.06) ppt and (0.58 ± 0.13) ppt in the UT (flight section IV) as shown in Figure 1, panel (a). The UT flight section IV is characterized by a high local thermal tropopause for mid-latitudinal conditions (above 15 km). Here, IO VMRs correlate well with low potential vorticity (PV) of the probed air masses as derived from ERA5. Surface-origin tracers from CLaMS indicate a large contribution of surface air from Central America and adjacent oceans to the IO-rich air in the UT.

Using ERA-Interim, Lauther et al. (2022) showed that air masses transported and uplifted by category 5 hurricane Maria were probed during this flight on 1 October 2017. Our back trajectory calculations indicate that the iodine-rich air masses were not only uplifted by hurricane Maria, but also that their last contact with the MBL (trajectory

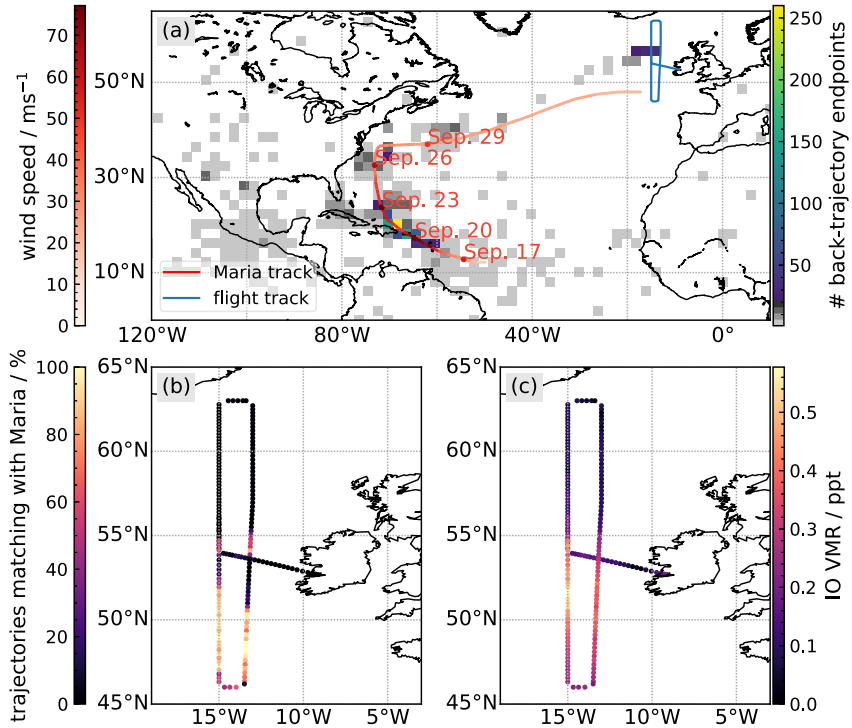

Figure 2. Panel (a) shows a heat map of back trajectory end points over 2° × 2° cells and the flight track of the research flight on 1 October 2017 (blue). Additionally, the track of hurricane Maria according to Pasch et al. (2019) is shown in red with the transparency indicating the maximum sustained surface wind speed. Panel (b) shows the percentage of "Maria-matching back trajectories" (out of 20 total back trajectories started within the averaging volume of each IO observation) along the flight track. If the distance between the hurricane and the trajectory endpoint is smaller than 200 km, the trajectory is classified as "Maria-matching back trajectory." The IO concentration along the flight track is shown in panel (c).

endpoints) has a distance of less than 200 km to the center of hurricane Maria at that time as shown in Figure 2. All back trajectories, whose endpoint fulfills this criterion are further called "Maria-matching back trajectories." These "Maria-matching back trajectories" thus are connected to an oceanic source region that was directly influenced by the hurricane, that is, high wind speeds and large scale updrafts (Cangialosi et al., 2021; Pasch et al., 2019) (see Figure 3 below). The percentage of trajectories (out of 20 back trajectories calculated within the averaging volume of each IO observation) matching with Maria is used to quantify the contribution of "Maria-matching back trajectories" to the probed air masses of each IO observation. Figures 2b and 2c show a remarkably strong correlation of the retrieved IO VMRs with the fraction of "Maria-matching back trajectories" (up to 100% for some observations).

Similar signatures of enhanced IO were detected in air masses probed on a flight that headed south from Ireland toward the Azores on 27 September 2017. For this flight, elevated IO ranged between (0.14 ± 0.06) ppt and (0.22 ± 0.06) ppt (mean: (0.18 ± 0.02) ppt) at flight altitudes between 11 and 14 km as shown in Figure S3 of Supporting Information S1 (later half of flight section II). Similar to the flight on 1 October 2017, the elevated IO coincides with the flight sections of low PV (below 3 PVU) and high local tropopause (around 15.5 km). For 27 September 2017, several dozen of the calculated back trajectory endpoints match temporally and spatially with the track of category 5 hurricane Irma, when it was located between Cuba and Florida, USA during the first half of September 2017. Again, we find a coincidence of iodine-rich air masses and "Irma-matching back trajectories", however, at most 45% of the back trajectories per IO observation match within 200 km distance to Irma (Figure S4 in Supporting Information S1). Furthermore, the transport time from the MBL to our measurement location was several days longer than for the iodine-rich air masses detected on 1 October 2017. The lower IO observed in Irma-influenced air masses is likely related to the smaller contribution of hurricane-processed air to the probed air masses. In addition, the several-days-longer transport time allows for increased air-mass mixing and a reduction of IO if inorganic iodine sinks exceed sources from iodocarbon destruction and iodine release from aerosol in the UT.

4. Discussion

Our observations provide compelling evidence that enhanced IO can be traced back to hurricane-processed air masses. Our retrieved background IO VMRs are consistent with previous studies in the marine FT, which attributed the widespread presence of IO to inorganic iodine recycling on aerosols (Dix et al., 2013; Koenig et al., 2020; Volkamer et al., 2015). Several studies have also reported on variable IO in the FT: Wang et al. (2015) reported on ∼0.04 to 0.28 ppt in the Eastern Pacific FT with the highest IO VMRs found in air influenced by marine deep convection; Lee et al. (2024) observed varying IO up to 0.15 ppt over the central continental US with the highest IO signals attributed to air masses originating from the subtropical Pacific with transport times lower than 24 h. Further, Schill et al. (2025) showed a strong variability in non-sea-salt aerosol iodine abundance over the mid-latitude Atlantic, with UT abundances ranging between ∼0.04 and ∼0.2 ppt.

Remarkably, IO found in aged hurricane-processed air masses on 1 October 2017 is up to a factor of 2–3 more than previously observed in air masses transported by marine deep convection into the tropical and subtropical FT (Dix et al., 2013; Wang et al., 2015). The level of IO observed on 27 September 2017 is consistent with that reported by Wang et al. (2015). More IO in the FT, up to ∼2 ppt, has only been observed inside lofted dust layers up to 6 km altitude (Koenig et al., 2021).

Three processes may contribute to the elevated IO observed in aged hurricane-influenced air masses: (a) strong emissions of iodinated compounds from the ocean, (b) fast vertical transport of these iodine-rich air masses into the UT, possibly involving little mixing with iodine-poor air, (c) physicochemical processing along the transport pathway, including recycling of iodine via aerosol-mediated photochemistry and wet removal.

Strong emissions of inorganic and organic iodine (a) can be motivated by the extreme surface wind speeds and gusts caused by hurricanes, which imply high friction velocities and thus enhanced air-sea gas exchange (see Text S3 in Supporting Information S1 for details on air–sea exchange at high wind speeds). For hurricanes Maria and Irma, reported maximum wind speeds reach ∼70–80 m s^{-1} (Cangialosi et al., 2021; Pasch et al., 2019). Since inorganic iodine emissions depend on the atmospheric O_3 deposition to the water, which increases with increasing wind speed (Helmig et al., 2012; Loades et al., 2020; Pound et al., 2024), enhanced production of I_2 and HOI in the surface waters is evident in hurricanes. The transport of these inorganic iodine products into the atmosphere competes with their transport into bulk oceanic water. At high wind speeds, the relative velocities of both transfers are currently uncertain resulting in an unquantified marine emission strength of inorganic iodine.

For lower winds (several m s^{-1}), Quack and Wallace (2003), Ziska et al. (2013), Tegtmeier et al. (2012), and Tegtmeier et al. (2013) argued that emissions of marine halocarbons (i.e., bromocarbons and CH_3I) increase with increasing wind speeds. Biogenic halocarbon emissions are also enhanced in biologically active ocean regions (e.g., coastal and upwelling areas), where algae and plankton are major sources. According to Ziska et al. (2013) and Booge et al. (2024), the Central American Atlantic is a source region of atmospheric CH_3I, but not a global hotspot.

In addition, the study of Troitskaya et al. (2017) indicates largely elevated generation of sea spray for fast winds, which may support efficient halogen recycling in hurricane-processed air masses but likely its relative contribution to the total iodine source strength is small (Moon et al., 2025).

Fast vertical transport (b) is demonstrated by the CLaMS back trajectories (Figure 3). Hurricane-processed air masses first experienced a rapid vertical uplift into the tropical UT within a few hours and then performed a several-week-long journey within the UT to mid-latitudes. The majority of air masses were uplifted by Maria, with smaller contributions of air masses uplifted by either hurricane Irma or category 4 hurricane Jose. An analysis of meteorological and transport parameters suggests a correlation of elevated IO with both, high 10 m wind gusts and high updraft velocities. Notably, both strong surface wind gusts and rapid vertical transport from the sea surface to the UT are favorable, but not sufficient for high IO found later in the UT. Similar results are obtained for the flight on 27 September 2017 (Figure S5 in Supporting Information S1). Further, the subsequent UT transport likely involved little mixing with background iodine-poor air, evidenced by sharp PV and θ gradients relative to surrounding air (Figure 1) (Konopka et al., 2007; Ploeger et al., 2015).

Additionally, the combined contribution of processes (a) and (b) is supported by the observation that several organic bromocarbons with primarily marine sources ($CHBr_3$, CH_2Br_2, CH_2BrCl, $CHBrCl_2$, and $CHBr_2Cl$) as well as total bromine (Br_y^{tot} were elevated in coincidence with elevated IO (Figure S6 in Supporting

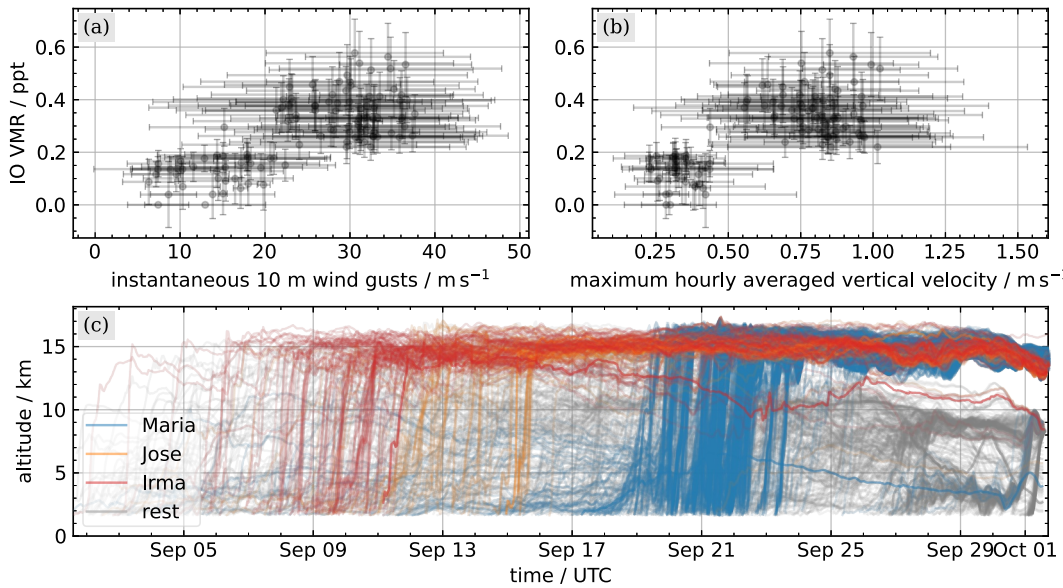

Figure 3. Analyzed meteorological and transport parameters for the flight on 1 October 2017 using ERA-5 reanalysis: panel (a) shows mean instantaneous 10 m wind gusts at the trajectories' MBL contact location and time as a function of inferred IO. Panel (b) shows mean maximum hourly averaged updraft velocities as a function of inferred IO. The data shows the mean and standard deviation of the respective velocities for all trajectories reaching the MBL within the 30 days prior to the measurements for each IO measurement. Panel (c) shows the trajectories' altitudes as function of time. Out of those trajectories with maximum hourly updrafts velocities > 0.5 ms^{-1}, 81% match with hurricane Maria (blue) within 300 km distance, another 6% match with hurricane Irma (red) and 5% with category 4 hurricane Jose (orange) (Berg, 2018). All other trajectories which did not match with one of those hurricanes are shown in gray.

Information S1) (Keber et al., 2020; Rotermund et al., 2021). Over the 2–3 weeks transport from the MBL, most CH_3I is expected to be photolyzed, although a small fraction may persist. This is consistent with elevated $CHBr_3$ and its comparable lifetime to CH_3I. Because bromocarbon enhancements are much smaller than the IO enhancements, we speculate that observed IO is dominated by inorganic iodine sources, with organic precursors playing a secondary role.

As pointed out by earlier studies, physicochemical processing (c), in particular aerosol-mediated recycling, is relevant to explain IO abundances in the FT (Dix et al., 2013; Koenig et al., 2020; Moon et al., 2025). MBL air masses experiencing high wind speeds should not be limited in sea salt aerosol providing surfaces for heterogeneous iodine reactions (Troitskaya et al., 2017; Li et al., 2022) which may prolong iodine lifetimes (Moon et al., 2025). Further, intermediately oxidized organics may also stimulate the release of iodine from aerosols (Huang et al., 2022; Reza et al., 2024).

During convective updraft, fractional wet removal of soluble iodinated gases (i.e., HOI, IO, OIO) and iodinated aerosols is also likely, since hurricane-induced upwelling produces strong precipitation (Guzman & Jiang, 2021). At higher altitudes, as the rising air strongly cools, soluble gases may be released back into the gas phase from freezing hydrometeors (Crutzen & Lawrence, 2000; Salzmann et al., 2007). Less soluble gases (e.g., CH_3I, I, I_2, INO_2, bromocarbons) and aerosols may survive the rapid vertical transport within the hurricane (Saiz-Lopez et al., 2014; Salzmann et al., 2007; Sander, 2023). Further, released and remaining gases undergo ice-recycling, which has been demonstrated to be necessary to reproduce measured FT IO abundances by models (Koenig et al., 2020; Moon et al., 2025).

During the subsequent week-long transport within the UT, photochemistry of the remaining iodinated gases and aerosols needs to establish the observed IO. The full physicochemical evolution of iodinated compounds along the trajectories can only be addressed by detailed modeling along the transport path, taking into account the complex meteorological conditions around hurricanes. Such a modeling framework is presently unavailable.

Within these iodine loaded air masses, conversion between gaseous inorganic iodine species is generally rapid and its speciation is largely dependent on O_3 concentrations. Using the speciation presented by Koenig

et al. (2020) at similar ozone concentrations, we infer a maximum total gaseous inorganic iodine $I_{y,gas}^{inorg} = (1.7 \pm 0.6)$ ppt (mean: $I_{y,gas}^{inorg} = (1.0 \pm 0.6)$ ppt) from our IO observations on 1 October 2017. However, Moon et al. (2025) demonstrate that modeled iodine speciation depends strongly on the inclusion of heterogeneous recycling processes, implying that robust $I_{y,gas}^{inorg}$ cannot be inferred from our measured IO.

Our observation of elevated IO in the UT does not provide sufficient information on the relative contribution of the discussed processes (a) to (b), because they lack information on the various relevant processes along the transport path and observations of different iodine species.

In comparison to previous iodine studies in recent (< 7 d) marine convective outflow (Dix et al., 2013; Wang et al., 2015), we observed significantly more IO in aged (> 8 d) hurricane outflow on 1 October 2017. Certainly, longer transport times allow higher fractional destruction of initial CH_3I. However, Koenig et al. (2020) argued that in their study the contribution of organic source gases to UT/LMS $I_{y,gas}^{inorg}$ was minor. Since updraft velocities in marine deep convection and tropical cyclones are similar (Heymsfield et al., 2010) while precipitation is likely stronger in tropical cyclones, we assume a similar (or even higher) efficiency of process (c) during convective updrafts in hurricanes compared to marine deep convection. In this respect, it is remarkable that we observed higher IO VMRs than in previous studies. Consequently, marine emission strengths of iodinated species (process (a)) may be higher under hurricane conditions than under marine deep convection, owing to stronger surface winds.

Furthermore, if the iodine- and bromine-rich air masses are transported into the stratosphere, for example, by isentropic transport across the tropical tropopause layer (TTL)/the mid-latitude LMS barrier (Birner & Bönisch, 2011; Levine et al., 2007) or by stratospheric-tropospheric exchange (STE) in the mid-latitudes, the iodine and bromine is readily available for stratospheric ozone depletion. The potential of tropical cyclones to transport tropospheric air masses into the LMS was previously discussed (Jordan et al., 2003; Li et al., 2021; Vogel et al., 2014). Indeed, some of the CLaMS modeled 14-d forward trajectories eventually lead into the LMS (see Figures S7 and S8 in Supporting Information S1), though we did not probe air masses rich in IO anywhere in the LMS. The latter could be due to wind-shear across the tropopause or that most of the gaseous iodine was already taken-up by aerosols (Koenig et al., 2020).

5. Conclusion

The present study reports on IO measurements of the mini-DOAS instrument aboard HALO during two flights of the WISE campaign over the North-Atlantic in autumn of 2017. On 1 October 2017, elevated IO (maximum 0.58 ppt, mean 0.36 ± 0.08 ppt) was detected in stretches of air masses characterized by a low PV and a high local tropopause (around 15 km) off-coast southwestern Ireland between 12 and 13 km altitude. During another flight on 27 September 2017, (0.18 ± 0.02) ppt mean IO was detected in air masses with similar characteristics north of the Azores Islands between 11 and 14 km altitude. Backward trajectories calculated with CLaMS indicated that these iodine-rich air masses originated from the MBL within a circle of 200 km radius from the center of the category 5 hurricanes Irma and Maria. Simultaneously with elevated IO, bromocarbons with marine sources (CH_2Br_2, $CHBr_3$, CH_2BrCl, $CHBrCl_2$, and $CHBr_2Cl$) were also elevated above the tropospheric "background" (Keber et al., 2020; Rotermund et al., 2021).

Our study provides compelling evidence that tropical cyclones, in particular hurricanes in the tropical Atlantic, drive enhanced halogen gas abundances in the UT, with IO levels exceeding those previously reported for marine deep convection (Wang et al., 2015). The longer lifetime of hurricanes compared to marine deep convection supports a prolonged influence on halogen transport into the UT and subsequent transport into the extratropics. Elevated IO in hurricane outflow is thus likely a result of strong iodine emission sources in the hurricane-influenced MBL, efficient and fast vertical transport, and physicochemical processing of iodinated gases and aerosols along the transport path, including aerosol-mediated photochemistry and wet removal. The UT abundance of other oceanic source gases (e.g., organic halogen gases, dimethyl sulfide, …) are likely also influenced by the proposed processes as demonstrated for dimethyl sulfide by Jiao et al. (2026). It is uncertain if the frequency of tropical cyclones will increase with climate change, however there is evidence that their intensity will increase globally (Bhatia et al., 2019, 2022; Knutson et al., 2020). Thus, category 5 hurricanes, such as Irma and Maria, as well as tropical storms over the oceans and their combined effect on the atmospheric halogen abundance may become more relevant in the future.

For a better understanding of tropical cyclone–driven gas exchange and vertical transport, and to better assess the global impact on atmospheric halogens and thus photochemistry, additional measurement and modeling studies are required. Comprehensive measurements of iodinated and brominated gases, both organic and inorganic, as well as particulate iodine and bromine in air masses influenced by tropical cyclones at different stages of their life cycle are essential for quantifying the contributions of individual source gases to the total burdens of atmospheric iodine and bromine. These studies should characterize air-sea gas exchange, the chemical evolution of the air masses, including wet scavenging and aerosol mediated-recycling processes and ultimately their impact on the atmospheric oxidation capacity.

Conflict of Interest

The authors declare no conflicts of interest relevant to this study.

Availability Statement

CLaMS surface-origin tracer simulations, for- and backward-trajectories as well as iodine oxide, total bromine and brominated VSLS VMRs and flight track information are available via Zenodo (https://doi.org/10.5281/zenodo.17608999) (Voss et al., 2025). The hurricane tracks and wind speeds are available from NOAA (https://www.nhc.noaa.gov/data/tcr/AL152017_Maria.pdf, last accessed: 16 October 2025; https://www.nhc.noaa.gov/data/tcr/AL112017_Irma.pdf, last accessed: 16 October 2025; https://www.nhc.noaa.gov/data/tcr/AL122017_Jose.pdf, last accessed: 19 January 2026) (Berg, 2018; Cangialosi et al., 2021; Pasch et al., 2019). The CLaMS model code can be downloaded from https://jugit.fz-juelich.de/clams/clams-git.git. The ERA5 data used here are available from the Copernicus Climate Change Service (https://doi.org/10.24381/cds.143582cf) (Hersbach et al., 2017).

Acknowledgments

We thank the entire WISE team and the DLR FX team for successfully performing the campaign. Specifically, we thank Andreas Zahn for providing the FAIRO O_3 data. We are grateful for the funding of the HALO aircraft and in particular to the contributions of the German Research Foundation (DFG; HALO-SPP 1294 under project number 316646266) to the various HALO missions and for the research Grants (DFG; Grant PF-384/7-1, PF384/9-1, PF-384/16-1, PF-384/17, PF-384/19, PF 384/24-1, PF-384/23-1, BU-2599/9-1, BU-2599/10-1, VO-1276/5-1, and VO-1276/7-1) in support of our measurements from the HALO aircraft. We thank the European Centre for Medium-Range Weather Forecasts (ECMWF) for providing the ERA5 reanalyses and the Jülich Supercomputing Centre (JSC; Research Centre Jülich, Germany) for the computing time on the supercomputer JUWELS (project CLaMS-ESM) and for the storage resources. The authors used ChatGPT (OpenAI) for language editing and coding support. All results, analysis, and conclusions were produced and verified by the authors. The authors gratefully acknowledge the data storage service SDS@hd supported by the Ministry of Science, Research and the Arts Baden-Württemberg (MWK) and the German Research Foundation (DFG) through Grant INST 35/1803-1 FUGG and INST 35/1804-1 LAGG. We thank the editor Lynn Russell and the two anonymous reviewers for their comments, which helped to improve the paper. Open Access funding enabled and organized by Projekt DEAL.

References

Aiuppa, A., Federico, C., Franco, A., Giudice, G., Gurrieri, S., Inguaggiato, S., et al. (2005). Emission of bromine and iodine from Mount Etna volcano. *Geochemistry, Geophysics, Geosystems*, *6*(8). https://doi.org/10.1029/2005gc000965

Atkinson, H. M., Huang, R.-J., Chance, R., Roscoe, H. K., Hughes, C., Davison, B., et al. (2012). Iodine emissions from the sea ice of the Weddell Sea. *Atmospheric Chemistry and Physics*, *12*(22), 11229–11244. https://doi.org/10.5194/acp-12-11229-2012

Badia, A., Reeves, C. E., Baker, A. R., Saiz-Lopez, A., Volkamer, R., Koenig, T. K., et al. (2019). Importance of reactive halogens in the tropical marine atmosphere: A regional modelling study using WRF-Chem. *Atmospheric Chemistry and Physics*, *19*(5), 3161–3189. https://doi.org/10.5194/acp-19-3161-2019

Bauer, D., Ingham, T., Carl, S. A., Moortgat, G. K., & Crowley, J. N. (1998). Ultraviolet-visible absorption cross sections of gaseous HOI and its photolysis at 355nm. *The Journal of Physical Chemistry A*, *102*(17), 2857–2864. https://doi.org/10.1021/jp9804300

Berg, R. (2018). *National Hurricane center tropical cyclone report: Hurricane Jose (AL122017)*. (Tech. Rep.). NOAA: National Hurrican Center. Retrieved from https://www.nhc.noaa.gov/data/tcr/AL122017_Jose.pdf

Bhatia, K., Baker, A., Yang, W., Vecchi, G., Knutson, T., Murakami, H., et al. (2022). A potential explanation for the global increase in tropical cyclone rapid intensification. *Nature Communications*, *13*(1), 6626. https://doi.org/10.1038/s41467-022-34321-6

Bhatia, K., Vecchi, G. A., Knutson, T. R., Murakami, H., Kossin, J., Dixon, K. W., & Whitlock, C. E. (2019). Recent increases in tropical cyclone intensification rates. *Nature Communications*, *10*(1), 635. https://doi.org/10.1038/s41467-019-08471-z

Birner, T., & Bönisch, H. (2011). Residual circulation trajectories and transit times into the extratropical lowermost stratosphere. *Atmospheric Chemistry and Physics*, *11*(2), 817–827. https://doi.org/10.5194/acp-11-817-2011

Bloss, W. J., Lee, J. D., Johnson, G. P., Sommariva, R., Heard, D. E., Saiz-Lopez, A., et al. (2005). Impact of halogen monoxide chemistry upon boundary layer OH and HO_2 concentrations at a coastal site. *Geophysical Research Letters*, *32*(6). https://doi.org/10.1029/2004GL022084

Booge, D., Tjiputra, J. F., Olivié, D. J., Quack, B., & Krüger, K. (2024). Natural marine bromoform emissions in the fully coupled ocean–atmosphere model NORESM2. *Earth System Dynamics*, *15*(3), 801–816. https://doi.org/10.5194/esd-15-801-2024

Bösch, H., Camy-Peyret, C., Chipperfield, M. P., Fitzenberger, R., Harder, H. U. P., & Pfeilsticker, K. (2003). Upper limits of stratospheric IO and OIO inferred from center-to-limb-darkening-corrected balloon-borne solar occultation visible spectra: Implications for total gaseous iodine and stratospheric ozone. *Journal of Geophysical Research*, *108*(D15), 4455. https://doi.org/10.1029/2002jd003078

Butz, A., Bösch, H., Camy-Peyret, C., Chipperfield, M. P., Dorf, M., Kreycy, S., et al. (2009). Constraints on inorganic gaseous iodine in the tropical upper troposphere and stratosphere inferred from balloon-borne solar occultation observations. *Atmospheric Chemistry and Physics*, *9*(18), 7229–7242. https://doi.org/10.5194/acp-9-7229-2009

Cangialosi, J. P., Latto, A. S., & Berg, R. (2021). *National Hurricane center tropical cyclone report: Hurricane Irma (AL112017)*. (Tech. Rep.). NOAA: National Hurrican Center. Retrieved from https://www.nhc.noaa.gov/data/tcr/AL112017_Irma.pdf

Carpenter, L. J., MacDonald, S. M., Shaw, M. D., Kumar, R., Saunders, R. W., Parthipan, R., et al. (2013). Atmospheric iodine levels influenced by sea surface emissions of inorganic iodine. *Nature Geoscience*, *6*(2), 108–111. https://doi.org/10.1038/ngeo1687

Clemens, J., Vogel, B., Hoffmann, L., Griessbach, S., Thomas, N., Fadnavis, S., et al. (2024). A multi-scenario Lagrangian trajectory analysis to identify source regions of the Asian tropopause aerosol layer on the Indian subcontinent in August 2016. *Atmospheric Chemistry and Physics*, *24*(1), 763–787. https://doi.org/10.5194/acp-24-763-2024

Crutzen, P. J., & Lawrence, M. G. (2000). The impact of precipitation scavenging on the transport of trace gases: A 3-dimensional model sensitivity study. *Journal of Atmospheric Chemistry*, *37*(1), 81–112. https://doi.org/10.1023/A:1006322926426

Deutschmann, T., Beirle, S., Frieß, U., Grzegorski, M., Kern, C., Kritten, L., et al. (2011). The Monte Carlo atmospheric radiative transfer model McArtim: Introduction and validation of Jacobians and 3D features. *Journal of Quantitative Spectroscopy & Radiative Transfer*, *112*(6), 1119–1137. https://doi.org/10.1016/j.jqsrt.2010.12.009

Dix, B., Baidar, S., Bresch, J. F., Hall, S. R., Schmidt, K. S., Wang, S., & Volkamer, R. (2013). Detection of iodine monoxide in the tropical free troposphere. *Proceedings of the National Academy of Sciences*, *110*(6), 2035–2040. https://doi.org/10.1073/pnas.1212386110

Engel, A., Rigby, M., Burkholder, J. B., Fernandez, R. P., Froidevaux, L., et al. (2018). *Update on ozone-depleting substances (ODS) and other gases of interest to the Montreal protocol, chapter 1 in scientific assessment of ozone depletion: 2018, global ozone research and monitoring project–report no. 58*. World Meteorological Organization, Geneve.

Finkenzeller, H., Iyer, S., He, X.-C., Simon, M., Koenig, T. K., Lee, C. F., et al. (2023). The gas-phase formation mechanism of iodic acid as an atmospheric aerosol source. *Nature Chemistry*, *15*(1), 129–135. https://doi.org/10.1038/s41557-022-01067-z

Grooß, J.-U., Müller, R., Crowley, J. N., & Hegglin, M. I. (2025). Chlorine peroxide reaction explains observed wintertime hydrogen chloride in the Antarctic vortex. *Communications Earth & Environment*, *6*(1), 1–8.

Guzman, O., & Jiang, H. (2021). Heavier inner-core rainfall of major hurricanes in the North Atlantic basin than in other global basins. *Journal of Climate*, *34*(14), 5707–5721. https://doi.org/10.1175/JCLI-D-20-0668.1

He, X.-C., Tham, Y. J., Dada, L., Wang, M., Finkenzeller, H., Stolzenburg, D., et al. (2021). Role of iodine oxoacids in atmospheric aerosol nucleation. *Science*, *371*(6529), 589–595. https://doi.org/10.1126/science.abe0298

Helmig, D., Lang, E. K., Bariteau, L., Boylan, P., Fairall, C. W., Ganzeveld, L., et al. (2012). Atmosphere-ocean ozone fluxes during the TEXAQS 2006, stratus 2006, GOMECC 2007, GASEX 2008, and AMMA 2008 cruises. *Journal of Geophysical Research*, *117*(D4). https://doi.org/10.1029/2011JD015955

Hersbach, H., Bell, B., Berrisford, P., Hirahara, S., Horányi, A., Muñoz-Sabater, J., et al. (2020). The ERA5 global reanalysis. *Quarterly Journal of the Royal Meteorological Society*, *146*(730), 1999–2049. https://doi.org/10.1002/qj.3803

Hersbach, H., Bell, B., Berrisford, P., Hirahara, S., Horányi, A., Muñoz-Sabater, J., et al. (2017). Complete ERA5 from 1940: Fifth generation of ECMWF atmospheric reanalyses of the global climate [Dataset]. *Copernicus Climate Change Service (C3S) Data Store (CDS)*. https://doi.org/10.24381/cds.143582cf

Heymsfield, G. M., Tian, L., Heymsfield, A. J., Li, L., & Guimond, S. (2010). Characteristics of deep tropical and subtropical convection from nadir-viewing high-altitude airborne Doppler radar. *Journal of the Atmospheric Sciences*, *67*(2), 285–308. https://doi.org/10.1175/2009JAS3132.1

Hoffmann, L., & Spang, R. (2022). An assessment of tropopause characteristics of the ERA5 and ERA-interim meteorological reanalyses. *Atmospheric Chemistry and Physics*, *22*(6), 4019–4046. https://doi.org/10.5194/acp-22-4019-2022

Huang, R.-J., Hoffmann, T., Ovadnevaite, J., Laaksonen, A., Kokkola, H., Xu, W., et al. (2022). Heterogeneous iodine-organic chemistry fast-tracks marine new particle formation. *Proceedings of the National Academy of Sciences*, *119*(32), e2201729119. https://doi.org/10.1073/pnas.2201729119

Hüneke, T. (2016). *The scaling method applied to HALO measurements: Inferring absolute trace gas concentrations from airborne limb spectroscopy under all sky conditions* (PhD). University of Heidelberg. Retrieved from https://katalog.ub.uni-heidelberg.de/cgi-bin/titel.cgi?katkey=68111443

Hüneke, T., Aderhold, O.-A., Bounin, J., Dorf, M., Gentry, E., Grossmann, K., et al. (2017). The novel halo mini-Doas instrument: Inferring trace gas concentrations from airborne UV/visible limb spectroscopy under all skies using the scaling method. *Atmospheric Measurement Techniques*, *10*(11), 4209–4234. https://doi.org/10.5194/amt-10-4209-2017

Jiao, G., Lou, S., Liu, T., Lin, H., Wang, X., Pan, L. L., et al. (2026). DMS uplift by tropical cyclones as a source of SO_2 in the upper troposphere. *Geophysical Research Letters*, *53*(7), e2025GL119981. https://doi.org/10.1029/2025GL119981

Jordan, C. E., Dibb, J. E., & Finkel, R. C. (2003). 10Be/7Be tracer of atmospheric transport and stratosphere-troposphere exchange. *Journal of Geophysical Research*, *108*(D8). https://doi.org/10.1029/2002JD002395

Keber, T., Bönisch, H., Hartick, C., Hauck, M., Lefrancois, F., Obersteiner, F., et al. (2020). Bromine from short-lived source gases in the extratropical northern hemispheric upper troposphere and lower stratosphere (UTLS). *Atmospheric Chemistry and Physics*, *20*(7), 4105–4132. https://doi.org/10.5194/acp-20-4105-2020

Klobas, J. E., Hansen, J., Weisenstein, D. K., Kennedy, R. P., & Wilmouth, D. M. (2021). Sensitivity of iodine-mediated stratospheric ozone loss chemistry to future chemistry-climate scenarios. *Frontiers in Earth Science*, *9*, 617586. https://doi.org/10.3389/feart.2021.617586

Kluge, F., Hüneke, T., Knecht, M., Lichtenstern, M., Rotermund, M., Schlager, H., et al. (2020). Profiling of formaldehyde, glyoxal, methylglyoxal, and CO over the Amazon: Normalised excess mixing ratios and related emission factors in biomass burning plumes. *Atmospheric Chemistry and Physics Discussions*, *2020*, 1–37. https://doi.org/10.5194/acp-2020-129

Kluge, F., Hüneke, T., Lerot, C., Rosanka, S., Rotermund, M. K., Taraborrelli, D., et al. (2023). Airborne glyoxal measurements in the marine and continental atmosphere: Comparison with TROPOMI observations and EMAC simulations. *Atmospheric Chemistry and Physics*, *23*(2), 1369–1401. https://doi.org/10.5194/acp-23-1369-2023

Knutson, T., Camargo, S. J., Chan, J. C. L., Emanuel, K., Ho, C.-H., Kossin, J., et al. (2020). Tropical cyclones and climate change assessment: Part II: Projected response to anthropogenic warming. *Bulletin of the American Meteorological Society*, *101*(3), E303–E322. https://doi.org/10.1175/BAMS-D-18-0194.1

Ko, M. K. W., Poulet, G., Blake, D. R., Boucher, O., Burkholder, J. H., et al. (2003). *Very short-lived halogen and sulfur substances, chapter 2 in scientific assessment of ozone depletion: 2002*. GAW Report, WMO, Geneva, No. 47.

Koenig, T. K., Baidar, S., Campuzano-Jost, P., Cuevas, C. A., Dix, B., Fernandez, R. P., et al. (2020). Quantitative detection of iodine in the stratosphere. *Proceedings of the National Academy of Sciences*, *117*(4), 1860–1866. https://doi.org/10.1073/pnas.1916828117

Koenig, T. K., Volkamer, R., Apel, E. C., Bresch, J. F., Cuevas, C. A., Dix, B., et al. (2021). Ozone depletion due to dust release of iodine in the free troposphere. *Science Advances*, *7*(52), eabj6544. https://doi.org/10.1126/sciadv.abj6544

Konopka, P., Günther, G., Müller, R., dos Santos, F. H. S., Schiller, C., Ravegnani, F., et al. (2007). Contribution of mixing to upward transport across the tropical tropopause layer (TTL). *Atmospheric Chemistry and Physics*, *7*(12), 3285–3308. https://doi.org/10.5194/acp-7-3285-2007

Lauther, V., Vogel, B., Wintel, J., Rau, A., Hoor, P., Bense, V., et al. (2022). In situ observations of CH_2Cl_2 and $CHCl_3$ show efficient transport pathways for very short-lived species into the lower stratosphere via the Asian and the North American summer monsoon. *Atmospheric Chemistry and Physics*, *22*(3), 2049–2077. https://doi.org/10.5194/acp-22-2049-2022

Lee, C. F., Elgiar, T., David, L. M., Wilmot, T. Y., Reza, M., Hirshorn, N., et al. (2024). Elevated tropospheric iodine over the central continental United States: Is iodine a major oxidant of atmospheric mercury? *Geophysical Research Letters*, *51*(17), e2024GL109247. https://doi.org/10.1029/2024gl109247

Levine, J. G., Braesicke, P., Harris, N. R. P., Savage, N. H., & Pyle, J. A. (2007). Pathways and timescales for troposphere-to-stratosphere transport via the tropical tropopause layer and their relevance for very short lived substances. *Journal of Geophysical Research*, *112*(D4). https://doi.org/10.1029/2005JD006940

Li, D., Vogel, B., Müller, R., Bian, J., Günther, G., & Riese, M. (2021). Tropical cyclones reduce ozone in the tropopause region over the western Pacific: An analysis of 18-year ozonesonde profiles. *Earth's Future*, *9*(2), 2020EF001635. https://doi.org/10.1029/2020EF001635

Li, Q., Tham, Y. J., Fernandez, R. P., He, X.-C., Cuevas, C. A., & Saiz-Lopez, A. (2022). Role of iodine recycling on sea-salt aerosols in the global marine boundary layer. *Geophysical Research Letters*, *49*(6), e2021GL097567. https://doi.org/10.1029/2021GL097567

Loades, D. C., Yang, M., Bell, T. G., Vaughan, A. R., Pound, R. J., Metzger, S., et al. (2020). Ozone deposition to a coastal sea: Comparison of eddy covariance observations with reactive air–sea exchange models. *Atmospheric Measurement Techniques*, *13*(12), 6915–6931. https://doi.org/10.5194/amt-13-6915-2020

McKenna, D. S., Grooß, J.-U., Günther, G., Konopka, P., Müller, R., Carver, G., & Sasano, Y. (2002). A new chemical Lagrangian model of the stratosphere (CLaMS) 2. Formulation of chemistry scheme and initialization. *Journal of Geophysical Research*, *107*(D15), ACH4-1–14. https://doi.org/10.1029/2000JD000113

McKenna, D. S., Konopka, P., Grooß, J.-U., Günther, G., Müller, R., Spang, R., & Orsolini, Y. (2002). A new chemical Lagrangian model of the stratosphere (CLaMS) 1. Formulation of advection and mixing. *Journal of Geophysical Research*, *107*(D16), ACH15-1–15. https://doi.org/10.1029/2000JD000114

Moon, A. R., Liu, L., Wang, X., Chan, Y.-C., Fritzmann, A., Pound, R., et al. (2025). Aerosol iodine recycling is a major control on tropospheric reactive iodine abundance. *EGUsphere*, *2025*, 1–52.

O'Dowd, C. D., Jimenez, J. L., Bahreini, R., Flagan, R. C., Seinfeld, J. H., Hämeri, K., et al. (2002). Marine aerosol formation from biogenic iodine emissions. *Nature*, *417*(6889), 632–636. https://doi.org/10.1038/nature00775

Pasch, R. J., Penny, A. B., & Berg, R. (2019). *National Hurricane center tropical cyclone report: Hurricane Maria (AL152017)*. (Tech. Rep.). NOAA: National Hurrican Center. Retrieved from https://www.nhc.noaa.gov/data/tcr/AL152017_Maria.pdf

Ploeger, F., Abalos, M., Birner, T., Konopka, P., Legras, B., Müller, R., & Riese, M. (2015). Quantifying the effects of mixing and residual circulation on trends of stratospheric mean age of air. *Geophysical Research Letters*, *42*(6), 2047–2054. https://doi.org/10.1002/2014GL062927

Ploeger, F., Diallo, M., Charlesworth, E., Konopka, P., Legras, B., Laube, J. C., et al. (2021). The stratospheric Brewer–Dobson circulation inferred from age of air in the ERA5 reanalysis. *Atmospheric Chemistry and Physics*, *21*(11), 8393–8412. https://doi.org/10.5194/acp-21-8393-2021

Pommrich, R., Müller, R., Grooß, J.-U., Konopka, P., Ploeger, F., Vogel, B., et al. (2014). Tropical troposphere to stratosphere transport of carbon monoxide and long-lived trace species in the chemical Lagrangian model of the stratosphere (CLaMS). *Geoscientific Model Development*, *7*(6), 2895–2916. https://doi.org/10.5194/gmd-7-2895-2014

Pound, R. J., Brown, L. V., Evans, M. J., & Carpenter, L. J. (2024). An improved estimate of inorganic iodine emissions from the ocean using a coupled surface microlayer box model. *Atmospheric Chemistry and Physics*, *24*(17), 9899–9921. https://doi.org/10.5194/acp-24-9899-2024

Pundt, I., Pommereau, J., Phillips, & Lateltin, E. (1998). Upper limit of iodine oxide in the lower stratosphere. *Journal of Atmospheric Chemistry*, *30*(1), 173–185. https://doi.org/10.1023/a:1006071612477

Quack, B., & Wallace, D. W. R. (2003). Air-sea flux of bromoform: Controls, rates, and implications. *Global Biogeochemical Cycles*, *17*(1). https://doi.org/10.1029/2002GB001890

Reza, M., Iezzi, L., Finkenzeller, H., Roose, A., Ammann, M., & Volkamer, R. (2024). Iodine activation from iodate reduction in aqueous films via photocatalyzed and dark reactions. *ACS Earth and Space Chemistry*, *8*(12), 2495–2508. https://doi.org/10.1021/acsearthspacechem.4c00224

Rotermund, M. K., Bense, V., Chipperfield, M. P., Engel, A., Grooß, J.-U., Hoor, P., et al. (2021). Organic and inorganic bromine measurements around the extratropical tropopause and lowermost stratosphere: Insights into the transport pathways and total bromine. *Atmospheric Chemistry and Physics*, *21*(20), 15375–15407. https://doi.org/10.5194/acp-21-15375-2021

Saiz-Lopez, A., Blaszczak-Boxe, C. S., & Carpenter, L. (2015). A mechanism for biologically induced iodine emissions from sea ice. *Atmospheric Chemistry and Physics*, *15*(17), 9731–9746. https://doi.org/10.5194/acp-15-9731-2015

Saiz-Lopez, A., Fernandez, R. P., Li, Q., Cuevas, C. A., Fu, X., Kinnison, D. E., et al. (2023). Natural short-lived halogens exert an indirect cooling effect on climate. *Nature*, *618*(7967), 967–973. https://doi.org/10.1038/s41586-023-06119-z

Saiz-Lopez, A., Fernandez, R. P., Ordóñez, C., Kinnison, D. E., Gómez Martín, J. C., Lamarque, J.-F., & Tilmes, S. (2014). Iodine chemistry in the troposphere and its effect on ozone. *Atmospheric Chemistry and Physics*, *14*(23), 13119–13143. https://doi.org/10.5194/acp-14-13119-2014

Saiz-Lopez, A., Plane, J. M. C., Baker, A. R., Carpenter, L. J., von Glasow, R., Gómez Martín, J. C., et al. (2012). Atmospheric chemistry of iodine. *Chemical Reviews*, *112*(3), 1773–1804. https://doi.org/10.1021/cr200029u

Saiz-Lopez, A., Saunders, R. W., Joseph, D. M., Ashworth, S. H., & Plane, J. M. C. (2004). Absolute absorption cross-section and photolysis rate of I_2. *Atmospheric Chemistry and Physics*, *4*(5), 1443–1450. https://doi.org/10.5194/acp-4-1443-2004

Salzmann, M., Lawrence, M. G., Phillips, V. T. J., & Donner, L. J. (2007). Model sensitivity studies regarding the role of the retention coefficient for the scavenging and redistribution of highly soluble trace gases by deep convective cloud systems. *Atmospheric Chemistry and Physics*, *7*(8), 2027–2045. https://doi.org/10.5194/acp-7-2027-2007

Sander, R. (2023). Compilation of henry's law constants (version 5.0.0) for water as solvent. *Atmospheric Chemistry and Physics*, *23*(19), 10901–12440. https://doi.org/10.5194/acp-23-10901-2023

Schäfler, A., Fix, A., & Wirth, M. (2021). Mixing at the extratropical tropopause as characterized by collocated airborne H_2O and O_3 LiDAR observations. *Atmospheric Chemistry and Physics*, *21*(6), 5217–5234. https://doi.org/10.5194/acp-21-5217-2021

Schill, G. P., Froyd, K. D., Murphy, D. M., Williamson, C. J., Brock, C. A., Sherwen, T., et al. (2025). Widespread trace bromine and iodine in remote tropospheric non-sea-salt aerosols. *Atmospheric Chemistry and Physics*, *25*(1), 45–71. https://doi.org/10.5194/acp-25-45-2025

Simpson, W. R., Brown, S. S., Saiz-Lopez, A., Thornton, J. A., & von Glasow, R. (2015). Tropospheric halogen chemistry: Sources, cycling, and impacts. *Chemical Reviews*, *115*(10), 4035–4062. https://doi.org/10.1021/cr5006638

Sinnhuber, B.-M., Sheode, N., Chipperfield, M. P., & Feng, W. (2009). The contribution of anthropogenic bromine emissions to past stratospheric ozone trends: A modelling study. *Atmospheric Chemistry and Physics*, *9*(8), 2863–2871. https://doi.org/10.5194/acp-9-2863-2009

Sive, B. C., Varner, R. K., Mao, H., Blake, D. R., Wingenter, O. W., & Talbot, R. (2007). A large terrestrial source of methyl iodide. *Geophysical Research Letters*, *34*(17). https://doi.org/10.1029/2007gl030528

Stutz, J., & Platt, U. (1996). Numerical analysis and error estimation of differential optical absorption spectroscopy measurements with least square fits. *Applied Optics*, *30*(30), 6041–6053.

Stutz, J., Werner, B., Spolaor, M., Scalone, L., Festa, J., Tsai, C., et al. (2017). A new differential optical absorption spectroscopy instrument to study atmospheric chemistry from a high-altitude unmanned aircraft. *Atmospheric Measurement Techniques*, *10*(3), 1017–1042. https://doi.org/10.5194/amt-10-1017-2017

Tegtmeier, S., Krüger, K., Quack, B., Atlas, E., Blake, D. R., Boenisch, H., et al. (2013). The contribution of oceanic methyl iodide to stratospheric iodine. *Atmospheric Chemistry and Physics*, *13*(23), 11869–11886. https://doi.org/10.5194/acp-13-11869-2013

Tegtmeier, S., Krüger, K., Quack, B., Atlas, E. L., Pisso, I., Stohl, A., & Yang, X. (2012). Emission and transport of bromocarbons: From the West Pacific Ocean into the stratosphere. *Atmospheric Chemistry and Physics*, *12*(22), 10633–10648. https://doi.org/10.5194/acp-12-10633-2012

Troitskaya, Y., Kandaurov, A., Ermakova, O., Kozlov, D., Sergeev, D., & Zilitinkevich, S. (2017). Bag-breakup fragmentation as the dominant mechanism of sea-spray production in high winds. *Scientific Reports*, *7*(1), 1614. https://doi.org/10.1038/s41598-017-01673-9

Vogel, B., Günther, G., Müller, R., Grooß, J.-U., Hoor, P., Krämer, M., et al. (2014). Fast transport from Southeast Asia boundary layer sources to northern Europe: Rapid uplift in typhoons and eastward eddy shedding of the Asian monsoon anticyclone. *Atmospheric Chemistry and Physics*, *14*(23), 12745–12762. https://doi.org/10.5194/acp-14-12745-2014

Vogel, B., Lauther, V., Köllner, F., Ekinci, F., Rolf, C., Strobel, J., et al. (2026). Continental and marine source regions contributing to the outflow of the Asian summer monsoon anticyclone during the Phileas campaign in summer 2023. *Atmospheric Chemistry and Physics*, *26*, 6283–6319. https://doi.org/10.5194/acp-26-6283-2026

Vogel, B., Müller, R., Günther, G., Spang, R., Hanumanthu, S., Li, D., et al. (2019). Lagrangian simulations of the transport of young air masses to the top of the Asian monsoon anticyclone and into the tropical pipe. *Atmospheric Chemistry and Physics*, *19*(9), 6007–6034. https://doi.org/10.5194/acp-19-6007-2019

Vogel, B., Volk, C. M., Wintel, J., Lauther, V., Clemens, J., Grooß, J.-U., et al. (2024). Evaluation of vertical transport in ERA5 and ERA-Interim reanalysis using high-altitude aircraft measurements in the Asian summer monsoon 2017. *Atmospheric Chemistry and Physics*, *24*(1), 317–343. https://doi.org/10.5194/acp-24-317-2024

Volkamer, R., Baidar, S., Campos, T. L., Coburn, S., DiGangi, J. P., Dix, B., et al. (2015). Aircraft measurements of BrO, IO, glyoxal, NO_2, H_2O, O_2–O_2 and aerosol extinction profiles in the tropics: Comparison with aircraft-/ship-based in situ and LiDAR measurements. *Atmospheric Measurement Techniques*, *8*(5), 2121–2148. https://doi.org/10.5194/amt-8-2121-2015

Voss, K., Vogel, B., Diederich, T., Engel, A., Grooß, J.-U., Keber, T., et al. (2025). Tropical cyclones drive enhanced inorganic iodine in the mid-latitude upper troposphere [Dataset]. *Zenodo*. https://doi.org/10.5281/zenodo.17608999

Wang, S., Schmidt, J. A., Baidar, S., Coburn, S., Dix, B., Koenig, T. K., et al. (2015). Active and widespread halogen chemistry in the tropical and subtropical free troposphere. *Proceedings of the National Academy of Sciences*, *112*(30), 9281–9286. https://doi.org/10.1073/pnas.1505142112

Weyland, B., Rosanka, S., Taraborrelli, D., Bohn, B., Zahn, A., Obersteiner, F., et al. (2025). Airborne remote sensing of nitrous acid in the troposphere: Potential sources of excess HONO. *EGUsphere*, *2025*, 1–56. https://doi.org/10.5194/egusphere-2025-5085

Wittrock, F., Müller, R., Richter, A., Bovensmann, H., & Burrows, J. P. (2000). Measurement of iodine oxide (IO) above Spitsbergen. *Geophysical Research Letters*, *27*(10), 1471–1474. https://doi.org/10.1029/1999gl011146

WMO (World Meteorological Organisation). (2022). *Scientific assessment of ozone depletion: 2022, global ozone research and monitoring project–report no. 278*. Geneve. (p. 509).

Wu, D., Du, J., Deng, H., Wang, W., Xiao, H., & Li, P. (2014). Estimation of atmospheric iodine emission from coal combustion. *International Journal of Environmental Science and Technology*, *11*(2), 357–366. https://doi.org/10.1007/s13762-013-0193-4

Zahn, A., Weppner, J., Widmann, H., Schlote-Holubek, K., Burger, B., Kühner, T., & Franke, H. (2012). A fast and precise chemiluminescence ozone detector for eddy flux and airborne application. *Atmospheric Measurement Techniques*, *5*(2), 363–375. https://doi.org/10.5194/amt-5-363-2012

Ziska, F., Quack, B., Abrahamsson, K., Archer, S. D., Atlas, E., Bell, T., et al. (2013). Global sea-to-air flux climatology for bromoform, dibromomethane and methyl iodide. *Atmospheric Chemistry and Physics*, *13*(17), 8915–8934. https://doi.org/10.5194/acp-13-8915-2013

References From the Supporting Information

Bogumil, K., Orphal, J., Homann, T., Voigt, S., Spietz, P., Fleischmann, O. C., et al. (2003). Measurements of molecular absorption spectra with the SCIAMACHY pre-flight model: Instrument characterization and reference data for atmospheric remote-sensing in the 230–2380 nm region. *Journal of Photochemistry and Photobiology A: Chem*, *157*(2), 167–184. https://doi.org/10.1016/S1010-6030(03)00062-5

Chance, K., & Kurucz, R. (2010). An improved high-resolution solar reference spectrum for Earth's atmosphere measurements in the ultraviolet, visible, and near infrared. *Journal of Quantitative Spectroscopy & Radiative Transfer*, *111*(9), 1289–1295. (Special Issue Dedicated to Laurence S. Rothman on the Occasion of his 70th Birthday.). https://doi.org/10.1016/j.jqsrt.2010.01.036

Danckaert, T., Fayt, C., Van Roozendael, M., De Smedt, I., Letocart, V., Merlaud, A., & Pinardi, G. (2012). QDOAS software user manual.

Deike, L., Zhou, X., Rustogi, P., Stanley, R. H., Reichl, B. G., Bushinsky, S. M., & Resplandy, L. (2025). A universal wind–wave–bubble formulation for air–sea gas exchange and its impact on oxygen fluxes. *Proceedings of the National Academy of Sciences*, *122*(38), e2419319122. https://doi.org/10.1073/pnas.2419319122

Dong, Y., Yang, M., Bell, T. G., Marandino, C. A., & Woolf, D. K. (2025). Asymmetric bubble-mediated gas transfer enhances global ocean CO_2 uptake. *Nature Communications*, *16*(1), 10595. https://doi.org/10.1038/s41467-025-66652-5

Fleischmann, O. C., Hartmann, M., Burrows, J. P., & Orphal, J. (2004). New ultraviolet absorption cross-sections of BrO at atmospheric temperatures measured by a time-windowing Fourier transform spectroscopy. *Journal of Photochemistry and Photobiology A: Chem*, *168*(1), 117–132. https://doi.org/10.1016/j.jphotochem.2004.03.026

Krall, K. E., Smith, A. W., Takagaki, N., & Jähne, B. (2019). Air–sea gas exchange at wind speeds up to 85 m s^{-1}. *Ocean Science*, *15*(6), 1783–1799. https://doi.org/10.5194/os-15-1783-2019

Obersteiner, F., Bönisch, H., Keber, T., O'Doherty, S., & Engel, A. (2016). A versatile, refrigerant- and cryogen-free cryofocusing – Thermodesorption unit for preconcentration of traces gases in air. *Atmospheric Measurement Techniques*, *9*(11), 5265–5279. https://doi.org/10.5194/amt-9-5265-2016

Platt, U., Stutz, J., Platt, U., & Stutz, J. (2008). *Differential absorption spectroscopy*. Springer.

Polyansky, O. L., Kyuberis, A. A., Zobov, N. F., Tennyson, J., Yurchenko, S. N., & Lodi, L. (2018). ExoMol molecular line lists XXX: A complete high-accuracy line list for water. *Monthly Notices of the Royal Astronomical Society*, *480*(2), 2597–2608. https://doi.org/10.1093/mnras/sty1877

Sala, S., Bönisch, H., Keber, T., Oram, D. E., Mills, G., & Engel, A. (2014). Deriving an atmospheric budget of total organic bromine using airborne in situ measurements from the western Pacific area during Shiva. *Atmospheric Chemistry and Physics*, *14*(13), 6903–6923. https://doi.org/10.5194/acp-14-6903-2014

Serdyuchenko, A., Gorshelev, V., Weber, M., Chehade, W., & Burrows, J. P. (2014). High spectral resolution ozone absorption cross-sections – Part 2: Temperature dependence. *Atmospheric Measurement Techniques*, *7*(2), 625–636. https://doi.org/10.5194/amt-7-625-2014

Spietz, P., Gómez Martín, J. C., & Burrows, J. P. (2005). Spectroscopic studies of the I_2/O_3 photochemistry: Part 2. Improved spectra of iodine oxides and analysis of the IO absorption spectrum. *Journal of Photochemistry and Photobiology A: Chemistry*, *176*(1), 50–67. https://doi.org/10.1016/j.jphotochem.2005.08.023

Thalman, R., & Volkamer, R. (2013). Temperature dependent absorption cross-sections of O_2–O_2 collision pairs between 340 and 630 nm and at atmospherically relevant pressure. *Physical Chemistry Chemical Physics*, *15*(37), 15371–15381. https://doi.org/10.1039/C3CP50968K